AMERICAN
METEOROLOGICAL
SOCIETY

Bulletin of the American Meteorological Society

EARLY ONLINE RELEASE

This is a preliminary PDF of the author-produced manuscript that has been peer-reviewed and accepted for publication. Since it is being posted so soon after acceptance, it has not yet been copyedited, formatted, or processed by AMS Publications. This preliminary version of the manuscript may be downloaded, distributed, and cited, but please be aware that there will be visual differences and possibly some content differences between this version and the final published version.

The DOI for this manuscript is doi: 10.1175/BAMS-D-16-0050.1

The final published version of this manuscript will replace the preliminary version at the above DOI once it is available.

If you would like to cite this EOR in a separate work, please use the following full citation:

Zhao, P., X. Xu, F. Chen, X. Guo, X. Zheng, L. Liu, Y. Hong, Y. Li, Z. La, H. Peng, L. Zhong, Y. Ma, S. Tang, Y. Liu, H. Liu, Y. Li, Q. Zhang, Z. Hu, J. Sun, S. Zhang, L. Dong, H. Zhang, Y. Zhao, X. Yan, A. Xiao, W. Wan, Y. Liu, J. Chen, G. Liu, Y. Zhaxi, and X. Zhou, 2017: The Third Atmospheric Scientific Experiment for Understanding the Earth-Atmosphere Coupled System over the Tibetan Plateau and Its Effects. Bull. Amer. Meteor. Soc. doi:10.1175/BAMS-D-16-0050.1, in press.

© 2017 American Meteorological Society

Manuscript (non-LaTeX) Click here to download Manuscript (non-LaTeX) Manuscript.docx

The Third Atmospheric Scientific Experiment for Understanding the Earth-Atmosphere Coupled System over the Tibetan Plateau and Its Effects

Ping Zhao[1, 2], Xiangde Xu[1], Fei Chen[1,3], Xueliang Guo[1], Xiangdong Zheng[1], Liping Liu[1], Yang Hong[4], Yueqing Li[5], Zuo La[6], Hao Peng[1], Linzhi Zhong[1], Yaoming Ma[7], ShihaoTang[8], Yimin Liu[9], Huizhi Liu[9], Yaohui Li[10], Qiang Zhang[11], Zeyong Hu[12], Jihua Sun[13], Shengjun Zhang[1], Lixin Dong[8], Hezhen Zhang[6], Yang Zhao[1], Xiaolu Yan[9], An Xiao[1], Wei Wan[14], Yu Liu[1], Junming Chen[1], Ge Liu[1], Yangzong Zhaxi[6], Xiuji Zhou[1]

[1]State Key Laboratory of Severe Weather, Chinese Academy of Meteorological Sciences, Beijing, China; [2]Collaborative Innovation Center on Forecast and Evaluation of Meteorological Disasters, Nanjing University of Information Science and Technology, Nanjing, China; [3]National Center for Atmospheric Research, Boulder, CO, United States; [4]National Weather Center and School of Civil Engineering and Environmental Sciences, University of Oklahoma, Norman, OK 73072, United States; [5]Chengdu Institute of Plateau Meteorology of the China Meteorological Administration, Chengdu, China; [6]Meteorological Bureau of Tibet Autonomous Region, Lhasa, China; [7]Institute of Tibetan Plateau Research of the Chinese Academy of Sciences, Beijing, China; [8]National Satellite Meteorological Center, Beijing, China; [9]Institute of Atmospheric Physics of the Chinese Academy of Sciences, Beijing, China; [10]Lanzhou Institute of Arid Meteorology of the China Meteorological Administration, Lanzhou, China; [11]Beijing Weather Modification Office, Beijing, China;[12]Cold and Arid Regions Environmental and Engineering Research Institute of the Chinese Academy of Sciences, Lanzhou, China; [13]Yunann Provincial Meteorological Bureau, Yunnan, China; [14]State Key Laboratory of Hydroengineering and Department of Hydraulic Engineering, Tsinghua University, Beijing, China.

Correspondence to: X. D. Xu (xuxd@camscma.cn) and P. Zhao (zhaop@cma.gov.cn).

PRELIMINARY ACCEPTED VERSION

Capsule Summary: Integrated monitoring systems for the land surface, boundary layer, troposphere, and lower stratosphere over the Tibetan Plateau promote the understanding of the earth-atmosphere coupled processes and their effects on weather and climate.

Abstract: This paper presents the background, scientific objectives, experimental design, and preliminary achievements of the Third Tibetan Plateau (TP) atmospheric scientific experiment (TIPEX-III) for eight to ten years. It began in 2013, and has expanded plateau-scale observation networks by adding observation stations in data-scarce areas, executed integrated observation missions for the land surface, planetary boundary layer, cloud-precipitation, and troposphere-stratosphere exchange processes by coordinating ground-based, air-based, and satellite facilities, and achieved noticeable progress in data applications. A new estimation gives a smaller bulk transfer coefficient of surface sensible heat over the TP, which results in a reduction of the overestimated heat intensity found in previous studies. Summer cloud-precipitation microphysical characteristics and cloud radiative effects over the TP are distinguished from those over the downstream plains. Warm rain processes play important roles in the development of cloud and precipitation over the TP. The lower-tropospheric ozone maximum over the northeastern TP is attributed to the regional photochemistry and long-range ozone transports, and the heterogeneous chemical processes of depleting ozone near the tropopause might not be a dominant mechanism for the summer upper tropospheric-lower stratospheric ozone valley over the southeastern TP. The TP thermodynamic function not only affects the local atmospheric water maintenance and the downstream precipitation and haze events, but also modifies extratropical atmospheric teleconnections like the Asian-Pacific Oscillation, subtropical anticyclones over the North Pacific and Atlantic, and

temperature and precipitation over Africa, Asia, and North America. These findings provide new insights into understanding land-atmosphere coupled processes over the TP and their effects, improving model parameterization schemes, and enhancing weather and climate forecast skills.

SCIENTIFIC BACKGROUND AND MOTIVATION.

The Tibetan Plateau (TP), known as the “sensible heat pump” and the “atmospheric water tower”, modifies monsoon circulations and regional energy and water cycles over Asia (Wu and Zhang 1998; Zhao and Chen 2001a; Wu et al. 2007; Xu et al. 2008b; Zhou et al. 2009). Strong ascent over the TP may transport lower-tropospheric water vapor and anthropogenic pollutants into the upper troposphere-lower stratosphere (UT-LS), which exerts an influence on the local ozone valley (Zhou et al. 1995; Liu et al. 2003; Bian et al. 2011) and the aerosol-layer enhancements near the tropopause (Tobo et al. 2007; Vernier et al. 2015). The TP also modulates large-scale atmospheric circulations over the Northern Hemisphere and atmosphere-ocean interactions in the tropics and mid-latitudes of the North Pacific (e.g., Zhao and Chen 2001b; Liu et al. 2007; Zhao et al. 2007; Nan et al. 2009; Zhao et al. 2009; Zhou et al. 2009; Duan et al. 2012). Therefore, global weather and climate research would be incomplete without considering the significant role of the TP.

Compared to other land regions in the world, observational data are scarce over the TP, owing to its high elevations, naturally harsh environmental conditions, and less-developed logistics. Thus, a few field experiments have been implemented in the data-scarce areas. For instance, the first Qinghai-Xizang Plateau Meteorology Experiment (QXPMEX) was carried out from May to August in 1979 (Tao et al. 1986). This experiment promoted, for the first time, systematic research on the diurnal and seasonal variations and spatial features of the surface heat budget, the structures and evolutions of atmospheric circulation systems over the TP, and their effects on global and Asian general circulations.

In the 1990s, a longer-term field experiment was conducted over the TP with the support of the Japanese Experiment on Asian Monsoon (JEXAM). It estimated the drag coefficient (C_d) of surface momentum and the bulk transfer coefficient (C_h) of surface sensible heat (*SH*), and revealed seasonal and interannual variations of the surface heat budget over the TP and their relationships with rainy seasons (Chen 1999; Zhao and Chen 2000a, b). Afterwards, the Second Tibetan Plateau Atmospheric Scientific Experiment (TIPEX-II) was carried out from May to August in 1998. Its results showed an imbalance phenomenon of the surface heat budget, strong mesoscale convection activities, and shear line characteristics (Chen et al. 1999). The GEWEX Asian Monsoon Experiment (GAME)/Tibet intensive observation conducted a plateau-scale automatic weather station experiment and a mesoscale experiment of the land surface and planetary boundary layer (PBL) observations with one X-band Doppler radar at Naqu from May to September in 1998 (Wang 1999; Ueno et al. 2001). GAME/Tibet made progress in retrieving the land surface radiative budget, precipitation, and soil moisture from satellite remote sensing products and understanding the PBL structures, the convective rapid development, and the precipitating cloud characteristics (Wang 1999; Ueno et al. 2001; Uyeda et al. 2001; Choi et al. 2004).

Entering the 21st century, the Coordinated Enhanced Observing Period (CEOP) Asia-Australia Monsoon Project on the Tibetan Plateau (CAMP/Tibet), and the Tibetan Observation and Research Platform (TORP) were implemented over the central northern TP during 2002–2004 (Ma et al. 2006, 2008). Their research documented regional characteristics of land-surface heat and CO_2 fluxes, turbulence, and the PBL (Ma et al. 2009). Under the support of the Japan International Cooperation Agency (JICA) project, a New Integrated Observational System over the Tibetan Plateau (NIOST) project (JICA/Tibet) was carried out during 2005–2009 (Xu et al. 2008a; Zhang et al. 2012; Chen et al. 2011, 2013). It found diurnal variations of rainfall over the TP and effects of latent heat release on the TP vortices, provided evidence of strong troposphere-stratosphere exchanges over the TP, improved the Noah land surface model on the basis of observational characteristics in the land surface energy balance, and revealed the importance of the deep PBL to the troposphere-stratosphere exchange over the TP. In the summer of 2011, an experiment of the TORP ground-based and airborne remote sensing observations was conducted over the central TP as part of the Global Change Program of China (Ma et al. 2014). This experiment found hydrothermal and momentum exchanges and moisture transports over the southeastern TP during the monsoon period, as well as land surface and atmospheric circulation variations against the background of global change. Moreover, the TiP program "Tibetan Plateau: Formation-Climate-Ecosystems" focused on a longer-term evolution of climate over the TP and its influence (Mosbrugger and Appel 2012).

To quantify uncertainties in satellite and model products of soil moisture and temperature, some regional-scale observation networks were established. For example, during 2008–2013 the CEOP-AEGIS (the Asian-monsoon systEm with Ground satellite Image data and numerical Simulations) project monitored the land surface characteristics and analyzed their linkages with convection, precipitation, and Asian monsoons by satellites, the existing ground-based flux measurements, and stable isotopes in precipitation over the southeastern TP (http://www.ceop-aegis.net/doku.php). The Tibetan Plateau observatory of plateau-scale soil moisture and soil temperature (Tibet-Obs) built a Naqu/Maqu/Ngari regional network in a cold semi-arid/cold humid/cold arid climate (Su et al. 2011). A regional-scale Soil Moisture and Temperature Monitoring Network (CTP-SMTMN) was also built on the central Tibetan Plateau (Yang et al. 2013). These field observation networks increased the understanding of regional land surface hydrological processes and errors of satellite-derived soil moisture products. In addition, an eco-hydrological experiment over the Heihe River basin in 2010 provided a test bed to confirm or falsify new ideas on eco-hydrology and new hypotheses on scaling (Li et al. 2013).

The aforementioned field experiments have made significant progress in promoting the scientific understanding of the earth-atmosphere coupled system over the TP. However, the problem of scarce observations in the area is still not well solved, which has further hindered the better understanding of the local land-atmosphere coupled system and its effects. The answers to some key scientific questions are still unclear. For example, owing to the lack of plateau-scale soil moisture and PBL observation networks, there is a wide divergence in estimates of C_d and C_h over the TP (e.g., Ye and Gao 1979; Zhao et al. 2000b; Choi et al. 2004; Gao et al. 2015; Zhang et al. 2016), which directly results in uncertainties when estimating the heat intensity and its impacts. Because of the lack of direct observations of cloud microphysical and troposphere-stratosphere exchange processes over the TP, the cloud microphysical characteristics in the formation and development of cloud and precipitation, their interactions with atmospheric environments, the UT-LS atmospheric vertical structures, and their effects on ozone variations and aerosol-layer enhancements near the tropopause are not well understood. Moreover, due to the scarce radiosonde data over the western TP, it is not known how the local atmospheric circulation systems (especially synoptic- and meso-scale systems) develop and move from the west to the east. Thus, numerical weather and climate forecast models often have poor reliability when modelling weather and climate features over the TP, including soil moisture, surface heat fluxes, surface air temperature, rainfall, PBL structures, cloud amount, and stratospheric ozone (Wang 2011; Wu and Zhou 2011;

Qiu et al. 2013; Hu et al. 2014; Zheng et al. 2014, 2015a, b, c, 2016; Guo et al. 2015; Zhuo et al. 2016; Wan et al. 2017). These problems may also cause large uncertainties in reanalysis datasets and satellite products (such as air temperature, soil moisture, surface heat fluxes, and radiation) over the TP (Li et al. 2012; Wang et al. 2012; Zhu et al. 2012; Su et al. 2013; Zeng et al. 2016).

To promote Tibetan meteorological research, the Third Tibetan Plateau Atmospheric Scientific Experiment (TIPEX-III), to continue for eight to ten years, was initiated jointly by the China Meteorological Administration (CMA), the National Natural Scientific Foundation of China (NSFC), and the Chinese Academy of Sciences (CAS). A preliminary experiment was implemented in 2013, and TIPEX-III began formally in 2014.

OBJECTIVES.

The field observational objective of TIPEX-III is to constitute a 3-D observation system of the land surface, PBL, troposphere, and lower stratosphere over the TP. This system integrates ground-, air-, and space-based platforms based on the meteorological operational networks, the TIPEX-III network, the existing NIOST network, and the part of the TORP observation sites in China. The scientific objectives of TIPEX-III are to understand the surface heat budget, cloud microphysical characteristics, atmospheric water cycles, and troposphere-stratosphere exchange characteristics over the TP; to clarify the impacts of the changing Tibetan land-atmosphere coupled system on severe weather and climate events and atmospheric energy and water cycles; to improve the parameterization schemes of the land surface, PBL, cloud-precipitation, and troposphere-stratosphere exchange processes over the TP; and to enhance the skills of weather and climate forecast operations. The specific intensive field observational and scientific objectives of TIPEX-III are addressed as follows:

(1) In the previous field experiments, the soil moisture and PBL networks were mainly located over the central and southeastern TP, not yet constituting a plateau-scale observation network. Meanwhile, the meteorological operational observation sites are still sparse from the western to central TP (Fig. 1a and b). To create plateau-scale soil moisture and PBL tower observation networks, TIPEX-III will build new sites over the data-scarce central and western areas, which may increase the understanding of temporal and spatial variations of the land surface characteristics over the TP, and their interactions with atmospheric circulations. Meanwhile, the regional-scale soil moisture and PBL networks over the TP will be used to understand mesoscale spatial differences in the surface heat budget over the complex topography and landscape, and their effects on mesoscale systems. These intensive observations also allow an objective evaluation of numerical models, reanalysis data, and satellite-retrieval products.

(2) The previous field experiments only utilized the X-band Doppler radar for probing large precipitating cloud particles, lacking direct observations of cloud microphysical features. TIPEX-III will carry out intensive observations over key areas with frequent cloud activities by integrating measurements of cloud radars, aircraft campaigns, and radiosondes, as well as regional-scale land-surface and PBL observation networks. These data will help to understand the microphysical characteristics of cloud development and interactions between clouds, surface heating, and atmospheric environments, and to improve parameterization schemes of cloud microphysical processes.

(3) The previous field experiments also lacked plateau-scale observations of troposphere-stratosphere exchange processes. TIPEX-III will conduct intensive observation tasks for water vapor, aerosol, and ozone in the troposphere and lower stratosphere by balloon-borne package instruments and ground-based remote sensing measurements. These data will help to clarify the UT-LS characteristics and the mechanisms for ozone variations and aerosol-layer enhancements near the tropopause; to validate satellite-retrieval profiles of water vapor, aerosol, and ozone, especially in the UT-LS; and to improve parameterization schemes of the lower-stratospheric physical and chemical processes over the TP.

(4) Only a few of the field experiments (such as the QXPMEX and TIPEX-II) executed intensive tropospheric radiosonde observations over the data-scarce western TP for about one year, not constituting a longer-term plateau-scale radiosonde observation network. To constitute such an observation network from the western to eastern TP, TIPEX-III will build new radiosonde stations over the western TP (Fig. 1b). These stations will gradually become part of the CMA operational observation system. The intensive observational data can be used to monitor the evolution of atmospheric circulation systems and water cycles from the west to the east, and may be applied in services of weather and climate forecasts.

(5) The importance of the summer TP "sensible heat pump" and "atmospheric water tower" to downstream monsoon rainfall has been documented (Wu and Zhang 1998; Xu et al. 2008b). However, their maintaining mechanisms and effects on the local atmospheric circulation systems, as well as extreme weather and climate events over the downstream area and a larger area of the Northern Hemisphere, are still not clearly understood. In particular, the dominant control of the South Asian monsoon by thermodynamic functions over the TP is controversial. Boss and Kuang (2010)

believed that the uplift of a narrow orography of the Himalayas and adjacent mountain ranges, instead of surface heating over the TP, plays a more important role in the South Asian monsoon climate. TIPEX-III will deeply investigate mechanisms responsible for the effects of the TP thermodynamic functions on the local atmospheric circulation systems and water cycles, and extreme weather and climate events in the downstream area, as well as the Northern Hemisphere, by multiple observational datasets and numerical simulations. TIPEX-III will also probe a way to enhance the skills of weather and climate forecasts.

Compared to the previous experiments, the unique feature of TIPEX-III is that it will greatly expand the surface and tropospheric meteorological operational observation networks over the traditionally data-scarce central and western parts of the TP, and promote integrated observations of multiple physical processes from the land surface to the lower stratosphere. Ultimately, the implementation of these observation networks could increase the understanding of the earth-atmosphere coupled system over the TP and its effects on extreme weather events and regional climate variability, and could also improve weather and climate forecast operations.

EXPERIMENTAL AREA AND NETWORK CONFIGURATION.

Considering the tremendous heterogeneity in terrain elevations and land cover types, the distributions of the existing CMA meteorological operational observation stations, and the logistical challenges of maintaining observation sites, TIPEX-III comprises a plateau-scale intensive observation network, as well as regional-scale dense networks (Fig. 1). With a particular focus on understanding the complex interactions between the land surface, PBL, and cloud microphysical processes over the TP, TIPEX-III also integrates intensive observations over a few areas with active convection using the regional-scale land-surface and PBL observation networks, ground-based radars, and airborne campaigns.

(a) Intensive observations of land-surface and PBL characteristics.

TIPEX-III has established a soil observation network consisting of 46 sites in the central and western TP (Fig. 1a). Consistent with the operational observations of the CMA, at each site the measurement system measures soil water content (Table 1). All of these sites have been operating since September 2015. Meanwhile, TIPEX-III has also built two regional-scale soil moisture and temperature observation networks over Shiquanhe—of the western bare soil with few features, and Naqu—of the central alpine steppe (Table 1 and Fig. 1a). The regional network consists of 33 sites over Naqu (Fig. 1c), which began operating in August 2015, and 17 sites over Shiquanhe (not shown), which began operating in December 2016.

For the PBL observations over the TP, TIPEX-III includes a plateau-scale network and a regional-scale network. The former consists of ten multi-layer towers (with distance between towers ~500 km) at Shiquanhe, Gaize, Naqu, Linzhou, Linzhi, Tuotuohe, Maqu, Litang, Dali, and Wenjiang (Fig. 1b and Table 1), and helps to study general patterns of the surface heat fluxes and PBL structures over the TP. The regional-scale network is located within an area of 300 km × 200 km near Naqu, a main source region of mesoscale low-pressure and convection systems over the TP. This network consists of six additional sites at Bange, Namucuo, Anduo, Nierong, Jiali, and Biru, and contributes to integrated research on the high-resolution land-surface and PBL processes over the central TP and their effects on mesoscale systems. These observations have been conducted at Shiquanhe, Namucuo, Naqu, Anduo, Linzhi, Litang, Dali, and Wenjiang from July 2014 to December 2016, at Bange, Biru, Jiali, and Nierong from July 2014 to March 2016, and at Linzhou from August 2015 to December 2016.

(b) Intensive routine radiosonde observations of tropospheric atmospheric profiles.

Using the Vaisala portable radiosonde systems (Table 2), TIPEX-III conducted the intensive routine radiosonde observations at Shiquanhe, Gaize, and Shenzha stations in the western TP (Fig. 1b) at 08:00 Beijing Standard Time (BST) (00:00 UTC), 14:00 BST, and 20:00 BST from July 8 to August 31 in 2014. Meanwhile, routine automatic sounding systems (Table 2) were newly built at these three stations, and have carried out intensive observations at 08:00 BST and 20:00 BST each day since November 2014. After assessment of their performance, these automatic sounding stations are to become part of the CMA operational observation systems, which will ultimately constitute a long-term plateau-scale sounding observation network. Moreover, TIPEX-III will also include intensive radiosonde observations at Gongshan (98.67°E, 27.75°N) station on the southeastern slope of the TP (Fig. 1b), a key area for gauging water-vapor transports from the Indian Ocean to East Asia.

(c) Intensive observations of tropospheric cloud-precipitation physical characteristics.

TIPEX-III combines ground-based radars (Table 3), aircraft campaigns (Table 4), and the CMA operational Doppler radar systems for measuring physical properties of cloud and precipitation in the central (Naqu) and southeastern TP (Linzhi and Daocheng) (Fig. 1b). A primary goal of these observations is to explore the cloud microphysical characteristics and their relationships with convective precipitation systems and atmospheric environments. In July and August 2014, a campaign by the ground-based radars and airborne instruments was conducted within a 200 km × 200 km area of Naqu (Fig. 1b). A follow-up field campaign using ground-based radars was carried out at Naqu and Linzhi from July 15 to August 31 in 2015, and at Daocheng from July 1 to August 31 2016.

(d) Intensive observations of troposphere-lower stratosphere ozone, aerosol, and water vapor profiles.

Strong transports of air masses from the troposphere to the lower stratosphere appear over the southeastern TP, and weaken toward the north and west (Tao et al. 1986; Cong et al. 2001). TIPEX-III includes plateau-scale intensive measurements for vertical profiles of ozone, aerosol, and water vapor at Shiquanhe, Lhasa, Linzhi, Tuotuohe, Mangya, Golmud, and Xining meteorological stations (Fig. 1b). Using balloon-borne package instruments and ground-based remote sensing instruments (Table 5), two observational missions were separately implemented at Linzhi from June 6 to July 31 in 2014 and at Shiquanhe, Lhasa, and Golmud during the period from May to September in 2016.

PRELIMINARY ACHIEVEMENTS OF TIPEX-III.

The implementation of TIPEX-III has enhanced the monitoring capability for the land surface, PBL, troposphere, and lower stratosphere over the TP. It has also promoted the understanding of their features, physical processes, and effects, and improved the capability of weather and climate models. Noticeable progress has been achieved in research and data applications.

(a) The new TIPEX-III data revealed an overestimation of the bulk transfer coefficient of sensible heat over the TP in previous studies, a larger plateau-scale heterogeneity in latent heat flux than in sensible heat flux, and the linkages of surface heat fluxes to Asian monsoon activities.

The plateau-scale heating contrasts exert a significant effect on the development of mesoscale convection and circulation systems over the eastern TP (Sugimoto and Ueno 2010). However, previous estimates of C_d, C_h, and surface heat fluxes show large uncertainties over the TP. The new data allowed the plateau-scale differences in C_d, C_h, and surface heat fluxes, to be re-examined. It was found that a new estimate of *SH* is 18 W m^{-2} in the central TP (with a range between 5 W m^{-2} and 40 W m^{-2}) and 56 W m^{-2} at the western TP (with a variation between 40 W m^{-2} and 70 W m^{-2}) (Fig. 2a). The spatial difference in *SH* is larger on the plateau scale (between the west and central parts) than on the regional scale (in the Naqu regional network); and surface latent heat flux (*LH*) has a larger plateau-scale difference than *SH* (Fig. 2b). The new estimate of C_h (2 to 4×10^{-3}) shows the larger plateau-scale heterogeneity relative to C_d (3 to 11×10^{-3}) (Table 6), and is smaller than previous estimates ($>4\times10^{-3}$) (e.g., Ye and Gao 1979; Yang and Guo 2011). Based on the larger values of C_h, the estimated July-August mean intensity of *SH* is 60-80 W m^{-2}/150-190 W m^{-2} over the central/western TP by Ye and Gao (1979), and 50-60 W m^{-2}/75-90 W m^{-2} by Yang and Guo (2011), remarkably larger compared to the new estimate. This result indicates that *SH* has been overestimated by the previous studies when calculating *SH* using the bulk transfer method, which could lead to an incorrect understanding of the TP *SH* intensity. Therefore, the role of summer *SH* over the TP in local thermal convective formation and development, and the uncertainties in model land surface processes, must be re-estimated. Moreover, it was also found that in the numerical forecast models, the overestimated "pumping effect" of summer *SH* over the TP may be reduced by improving the parameterization scheme of land surface processes for bare soil (Zhuo et al. 2016).

The data diagnosis of TIPEX-III further revealed a plateau-scale difference in diurnal variations of surface heat fluxes over the TP, and their linkages with the South Asian monsoon. *SH* shows a larger diurnal variation in the west than in the middle and east, but *LH* does not show remarkable diurnal variations (Wang et al. 2016). When the strong warm-moist southerly wind in front of the South Asian monsoon trough prevails over the southeastern TP, the diurnal variations of local *SH* and downward shortwave radiation are weaker (Li et al. 2016), which suggests the feedback of the Asian monsoon on the TP heat source. Previous studies paid more attention to the impacts of the TP heating on the Asian monsoon (e.g., Wu and Zhang 1998; Zhao and Chen 2001a, b; Liu et al. 2007; Zhou et al. 2009; Duan et al. 2012) or the effects of extratropical atmospheric planetary-scale waves over the Northern Hemisphere on the TP heating (Zhao et al. 2009; Cui et al. 2015). Thus this feedback of the Asian monsoon provides a new insight for understanding reasons for the TP heating variations.

(b) The new TIPEX-III observations uncovered the characteristics of cloud, its radiative effect, and raindrop size distribution, and the importance of warm rain processes in the formation and development of cloud and precipitation.

(1) Cloud diurnal variation and warm rain process.

The lack of direct observations for cloud physical processes hinders the understanding of the cloud microphysical characteristics over the TP and their roles in local cloud development. The TIPEX-III intensive observations revealed the diurnal variation of cloud over the TP. It was found that convective cloud and precipitation exhibits a distinct diurnal variation over the central TP. The strong convective precipitation begins at noon (Chang and Guo 2016), corresponding well to the peak of the local sensible heat flux (Wang et al. 2016), which implies an influence of surface heating on the diurnal variation of convection and precipitation. Convective precipitation then gradually turns to stratiform precipitation. For the stratiform cloud, the dominant cloud particles are raindrop-size supercooled water with fewer ice particles (Fig. 3a), which indicates a warm rain process. This process can generate heavier precipitation over the precipitation centers of weak convection systems than the cold rain processes (Gao et al. 2016).

(2) Characteristics of raindrop size distribution.

The new observational results indicate that the raindrop size distribution (RSD) over the TP is wider during the day than at night, with the widest RSD in the late afternoon (Chang and Guo 2016). Moreover, the RSD is wider over the TP compared to heavy rainfall over the downstream plains, and the concentration of cloud droplets is much lower compared to clean oceans. The RSD varies between 10^2 m^{-3} mm^{-3} and 10^3 m^{-3} mm^{-3} over the TP when the precipitation particle radius is <1 mm (Fig. 3b), and shows a Γ distribution when the radius is <2 mm. The larger raindrops (with a size of 10 μm) in the shallow convection over the TP (Fig. 3c) may enhance collision-coalescence processes, producing light rain, even though the concentration of larger raindrops is relatively low. This phenomenon is quite different from the plain of China where light rain is often suppressed by high aerosol loading. Because the atmospheric environment is relatively clean over the TP, the study of the formation and development of local cloud and precipitation could help to improve understanding of the effects of aerosols in a polluted atmospheric environment.

(3) Vertical structures of cloud radiative effect.

The TIPEX-III analysis with the CloudSat/CALIPSO products indicated a salient difference in the vertical structures of both shortwave and longwave cloud radiative effects (CRE) over the TP from the adjacent regions. This difference is characterized by the deeper shortwave CRE heating and longwave CRE cooling layers in the troposphere, and the maximum values of the CRE heating and cooling in the lower layers over the TP (Yan et al. 2016). A strong cooling layer of net CRE appears in the upper troposphere, and a shallow, but strong, heating layer appears in the lower layer. However, more general and precise information related to their full diurnal cycles and averages is needed to combine with the geostationary satellites and ground-based observations.

(c) The TIPEX-III observations and analyses revealed the contributions of regional photochemistry and long-range ozone transport to the lower-tropospheric ozone, and the relative importance of heterogeneous chemical processes near the tropopause and convective transports to the UT-LS ozone.

Because of lacking direct observational evidence for contributions of regional photochemistry reactions and horizontal and vertical transports to tropospheric and lower stratospheric ozone variations, the intensive observations of TIPEX-III helped to improve understanding of the contributions of these processes. It was found that, over the southeastern TP, the ozone concentration is lower in the middle and lower troposphere compared to the South Asian monsoon region, such as New Delhi, India (Fig. 4b). This lower-tropospheric low ozone over the TP could be mainly attributed to the lower anthropogenic pollution emissions through photochemical ozone production in the area. Over the northeastern TP, the lower-tropospheric ozone maximum could be attributed to both the regional photochemistry processes, and the long-range ozone transport from East Asia, Europe, and Africa during the summer (Zhu et al. 2016). Especially in June, the contribution of the regional photochemistry process is almost half of that of the horizontal transport.

Previous studies did not explicitly indicate the relative importance of upward transport from the lower-tropospheric low ozone concentration or in-situ photochemical processes caused by anthropogenic pollution emissions to the UT-LS ozone valley during the summer. The intensive profile observations of the TIPEX-III campaign over the southeastern TP revealed a mean temperature of >-78.15°C (the maximum temperature required for the formation of polar stratospheric clouds) and a low water vapor concentration near the tropopause (Fig. 4a), which indicates a dehydration process induced by a cold temperature trap. In such an environment, phenomena such as polar stratospheric clouds are not likely to occur over the TP, and the heterogeneous chemical reaction of depleting ozone is weak over the TP. Thus, the in-situ heterogeneous chemical processes near the tropopause might not be a dominant mechanism responsible for the formation of the UT-LS ozone valley during the summer.

Another mechanism, strong convective transports of the lower-tropospheric low ozone concentration toward the UT-LS, may have had a greater influence. Over the southeastern TP, the upward transports are closely associated with the strongest ascending motion. Under the influence of the plateau surface thermodynamic forcing, the upward transports are stronger in the daytime and summer. The tropopause fold is also a favorable structure for cross-tropopause exchanges. It is known as a vertical intrusion of the dynamical tropopause into the troposphere, and is accompanied by the normal tropopause break and two tropopause heights (that is, the polar tropopause height and the tropical tropopause height). The intensive observations of TIPEX-III revealed that the late rainy season is an important period for troposphere-stratosphere exchanges over the TP (Hong et al. 2016). In this season, the tropopause fold is frequently observed over the western TP. The polar tropopause occurs during the entire rainy season, but its height decreases from the early to late rainy season (Fig. 4c); while the tropical tropopause is mainly observed in the late rainy season (Fig. 4d), which is possibly associated with weaker upper-tropospheric jet streams over the western TP. The frequent occurrence of the tropopause fold favors the cross-tropopause exchange of air masses with different ozone concentrations between the troposphere and stratosphere. Meanwhile, the lower-tropospheric pollutants over the TP and its surrounding areas may have also been transported to the UT-LS, which could further affect the chemical processes of the UT-LS, as well as ozone concentrations. Thus, the effects of the increasing aerosol concentration near the tropopause over South Asia on chemical processes and ozone should be closely examined.

(d) The TIPEX-III analyses provided a new insight into the effects of the TP thermodynamic functions on local atmospheric water maintenance and vortex movement, downstream rainfall and haze events, and northern hemispheric continent temperature and rainfall.

The physical diagnoses and numerical simulations of TIPEX-III gave a maintenance mechanism responsible for the TP "atmospheric water tower". When the TP surface heating draws the warm-moist air masses from the tropical Indian Ocean toward the plateau, they travel along the southern slope of the TP, and form two ladders of the CISK (the conditional instability of the second kind) processes with two couplings of apparent heat source/moisture sink over the TP southern slope and main platform, respectively. This feature enforces the convergence of low-level low-pressure and convection systems over the platform and favors the formation and development of local cloud and precipitation (Fig. 5a). In this way, the TP “atmospheric water tower” is maintained (Xu et al. 2014).

The analyses of TIPEX-III also revealed new influence mechanisms for downstream extreme weather and climate events. It was found that when the extratropical westerlies climb over the TP, they descend on the lee side of the TP, which favors a near-surface “harbor” with weak wind over central-eastern China, followed by the accumulation of local air pollutants and the occurrence of extreme haze events (Xu et al. 2016). Moreover, the atmospheric heating intensity over the TP affects the movement of low-level vortices from the central to eastern TP (Li et al. 2014). In the developing stages of these vortices, the vertical structure of the heat source may determine their intensity and movement direction. The vortices moving away from the plateau usually trigger heavy rainfall to the east of the TP, and even give rise to disastrous rainfall events over downstream areas.

These results provide valuable information about the skills of downstream weather and climate forecasts. For example, improving the land surface and PBL processes over the TP in numerical forecast models can reduce an overestimated *SH* “pumping effect” and a cold bias in the land surface temperature over the TP, so the models can better capture the characteristics of precipitation over central-eastern China and the coasts (Zhuo et al. 2016). Moreover, TIPEX-III also uncovered that when the new intensive radiosonde data at Shiquanhe, Gaize, and Shenzha stations of the western TP are assimilated in the mesoscale WRF model system with three-dimensional variational data assimilation, the forecast skill of rainfall in the TP and adjacent areas is remarkably enhanced, with a decrease in the root mean square error of the 24-hour forecast rainfall by 11% over the TP (Fig. 5b).

TIPEX-III demonstrated an important modulation of the TP heating on large-scale atmospheric waves, teleconnections, and climates. *SH* and atmospheric latent heating over the TP could enhance the meridional circulation of the Asian summer monsoon, produce eastward-propagating Rossby waves along the extratropical westerlies, and modify large-scale climates over the Northern Hemisphere (Wu et al. 2016). TIPEX-III also discovered that during summer a strong surface heating over the TP could trigger a northern hemispheric extratropical teleconnection like the Asian-Pacific Oscillation (APO) (Liu et al. 2015, 2017), with an increased tropospheric temperature and strengthened ascent over Asia, and a decreased tropospheric temperature and strengthened descent over the central-eastern North Pacific (Fig. 5c). It has been known that associated with APO are significant anomalies in lows over the Asian-African monsoon region and subtropical anticyclones over the North Pacific and Atlantic, as well as surface air temperature and rainfall over Africa, South Asia, East Asia, and extratropical North America (Zhao et al. 2012). TIPEX-III further reveled that these APO-related anomalies in atmospheric circulation, rainfall, and temperature could be also forced by an individual surface heating change over the TP (Fig. 5d, e, and f), which suggests the importance of the TP forcing to global-scale climate anomalies, which should be further explored.

SUMMARY AND DISCUSSION.

Metrological observational data are scarce over the TP. Although a few field experiments over the TP have made significant progress, they have mostly focused on land surface and PBL observations. Routine surface and tropospheric observation stations are still sparse over the western TP. There is a lack of direct observations of cloud microphysical and troposphere-stratosphere exchange characteristics. All of these hinder the better understanding of the TP earth-atmosphere coupled system and its effects.

To promote Tibetan meteorological research, the CMA, NSFC, and CAS jointly initiated TIPEX-III for eight to ten years in 2013. It has been implemented as an integrated observation of the land surface, PBL, troposphere, and lower stratosphere by coordinating ground-, air-, and space-based facilities from the CMA operational networks and previous scientific experiment observation networks in China. The implementation of TIPEX-III has greatly expanded the CMA operational observation networks, and provided important support for the NSFC comprehensive research program during 2013–2022 entitled "The Earth-Atmosphere Coupled System over the Tibetan Plateau and Its Global Climate Effects".

TIPEX-III has achieved noticeable progress in research and data application. Its preliminary achievements provide a special reference to advance the understanding of the plateau land-atmosphere coupling system, as well as new insight into how to improve model physical parameterization schemes and enhance the skills of weather and climate forecasts. In the future, TIPEX-III will include further field experiments, and comprehensively study interactions between tropospheric cloud-precipitation physical processes, surface heating, and atmospheric environments over the TP. It will involve further examination of the vegetated surface aerodynamic conductance in land surface models and the importance of the heat source intensity over the TP to monsoon onsets and global and regional extreme weather and climate events; improve parameterization schemes of the land-surface, PBL, cloud-precipitation, and troposphere-stratosphere exchange processes over the TP; and validate assimilated and remote sensing products of soil temperature and moisture, and atmospheric ozone, aerosol, and water vapor.

Equally importantly, TIPEX-III aims to promote scientific exchanges and collaborations with international research communities and broader organizations. Coordinated observational experiments in the countries neighboring the TP are especially encouraged. Scientists from international communities are invited to participate in the follow-up field campaigns and to use the TIPEX-III data in their research. Validated TIPEX-III datasets will be open to the domestic and international scientific communities after a data-protection period of one year (starting from the dates of completion of the data quality control or the product generation). A dedicated data-archival center of the CMA, the National Meteorological Information Center (NMIC), is responsible for collecting the raw and processed datasets and distributing them to users. The website for downloading the TIPEX-III data (http://data.cma.cn/tipex) has been preliminarily built and will be further improved. Users are also encouraged to directly contact the corresponding authors of this paper (xuxd@camscma.cn; zhaop@cma.gov.cn) to obtain data and further details.

ACKNOWLEDGEMENTS. We thank all members of the TIPEX-III lead group, expert group, implementation group, and management office for their dedication and constructive suggestions. We thank the meteorologists of the Meteorological Bureau of Tibet Autonomous Region for their participation in field experiments. We thank Dr. Yunchang Cao of the Meteorological Observation Center of the CMA for his participation in the construction of automatic radiosonde stations, Drs. Zheng Ruan, Zhiqun Hu, Zehu Cui, and Wei Zhuang of the Chinese Academy of Meteorological

Sciences (CAMS) for their participation in ground-based radar observations, and Yang Gao and Delong Zhao of the Beijing Weather Modification Office and Dr. Guangxian Lu of CAMS for their participation in aircraft campaigns. This work is jointly sponsored by the Third Tibetan Plateau Atmospheric Experiment (GYHY201406001) and NSFC (91437218, 91537211, 91637312).

REFERENCES

Bian, J., R. Yan, H. Chen, D. Lu, and T. M. Steven, 2011: Formation of the summertime ozone valley over the Tibetan Plateau: The Asian summer monsoon and air column variations. *Adv. Atmos. Sci.*, **28**, 1318–1325.

Boos, W. R., and Z. M. Kuang, 2010: Dominant control of the South Asian monsoon by orographic insulation versus plateau heating. *Nature*, **463**, 218–223.

Chang, Y., and X. Guo, 2016: Characteristics of convective cloud and precipitation during summer time at Naqu over Tibetan Plateau (in Chinese). *Chinese Sci. Bull.*, **61**, 1706–1720.

Chen, L. S., X. Xu, and S. Yu, 1999: The second Tibetan Plateau field experiment: Air-land process and planetary boundary layer observational study. *Annual report of CAMS*, Beijing: Chinese Academy of Meteorological Sciences, pp15–17.

Chen, L. X., 1999: China-Japan cooperative research on Asian monsoon mechanisms. *Annual report of CAMS*, Beijing: Chinese Academy of Meteorological Sciences, pp26–28.

Chen X, J. A. Anel, Z. Su, L. Torre, H. Kelder, J. Peet, and Y. Ma, 2013: The deep atmospheric boundary layer and its significance to the stratosphere and troposphere exchange over the Tibetan Plateau. *PLOS ONE*, **8**, e56909, doi: 10.1371/journal.pone.0056909.

Chen, X., Y. Ma, H. Kelder, Z. Su, and K. Yang, 2011: On the behaviour of the tropopause folding events over the Tibetan Plateau. *Atmos. Chem. Phys.*, **11**, 5113–5122.

Choi, T., and Coauthors, 2004: Turbulent exchange of heat, water vapor, and momentum over a Tibetan prairie by eddy covariance and flux variance measurements. *J. Geophys. R*es., **109**, D21106, doi: 10.1029/2004JD004767.

Cong, C., W. L. Li, and X. Zhou, 2001: Mass exchange between the stratosphere and troposphere over the Tibetan Plateau and its adjacent region. *Chinese Sci. Bull.*, **46**, 1914–1918.

Cui, Y. F., A. M. Duan, Y. M. Liu, and G. X. Wu, 2015: Interannual variability of the spring atmospheric heat source over the Tibetan Plateau forced by the North Atlantic SSTA. *Clim. Dyn.*, **45**, 1617-1634.

Duan, A. M., G. X. Wu, Y. M. Liu, Y. M. Ma, and P. Zhao, 2012: Weather and climate effects of the Tibetan Plateau. *Adv. Atmos. Sci.*, **29**, 978–992.

Gao, W., C. Sui, J. Fan, Z. Hu, and L. Zhong, 2016: A study of cloud microphysics and precipitation over the Tibetan Plateau by radar observations and cloud-resolving model simulations. *J. Geophys. Res. Atmos.*, **121**, 13735–13752.

Gao, Y., K. Li, F. Chen, Y. Jiang, and C. Lu, 2015: Assessing and improving Noah-MP land model simulations for the central Tibetan Plateau. *J. Geophys. Res. Atmos.*, **120,** 9258–9278.

Guo, D., Y. Su, C. Shi, J. J. Xu, and A. M. Powell, 2015: Double core of ozone valley over the Tibetan Plateau and its possible mechanisms. *J. Atmos. Sol.-Terr. Phy.*, **130–131**, 127–131.

Hong, J., J. Guo, J. Du, and P. Wang, 2016: an observational study on the vertical structure of the upper troposphere and lower stratosphere in Gaize, Tibet during the rainy season (in Chinese). *Acta Meteor. Sin.*, **74**, 827–836.

Hu, Q., D. Jiang, and G. Fan, 2014: Evaluation of CMIP5 models over the Qinghai-Tibetan Plateau (in Chinese). *Chinese J. Atmos. Sci.*, **38**, 924–938.

Li, J., Y. Li, X. Jiang, and D. Gao, 2016: Characteristics of land-atmosphere energy exchanges over complex terrain area of southeastern Tibetan Plateau under different weather conditions (in Chinese). *Chinese J. Atmos. Sci.*, **40**, 777–791.

Li, L., R. Zhang, M. Wen, and L. Liu, 2014: Effect of the atmospheric heat source on the development and eastward movement of the Tibetan Plateau vortices. *Tellus A*, **66**, 419–439.

Li, R., S. H. Lv, B. Han, and Y. Gao, 2012: Preliminary comparison and analyses of air temperature at 2 m height between three reanalysis data-sets and observation in the East of Qinghai-Xizang Plateau (in Chinese). *Plateau Meteorology*, **31**, 1488–1502.

Li, X., and Coauthors, 2013: Telemetry experimental research (HiWATER) — Scientific objectives and experimental design. *Bull. Am. Meteor. Soc.*, **94**, 1146–1160.

Liu, G., P. Zhao, and J. Chen, 2017: Possible effect of the thermal condition of the Tibetan Plateau on the interannual variability of the summer Asian-Pacific Oscillation. *J. Climate*, doi: 10.1175/JCLI-D-17-0079.1.

Liu, G., P. Zhao, J. Chen, and S. Yang, 2015: Preceding factors of summer Asian–Pacific Oscillation and the physical mechanism for their potential influences. *J. Climate*, **28**, 2531–2543.

Liu, Y., B. J. Hoskins, and M. Blackburn, 2007: Impact of Tibetan orography and heating on the summer flow over Asia. *J. Met. Soc. Japan*, **85B**, 1–19.

Liu, Y., W. L. Li, X. Zhou, and J. He, 2003: Mechanism of formation of the ozone valley over the Tibetan plateau in summer-transport and chemical process of ozone. *Adv. Atmos. Sci.*, **20**, 103–109.

Ma, Y., and Coauthors, 2014: Study progresses of the Tibet Plateau climate system change and mechanism of its impact on East Asia (in Chinese). *Adv. Earth Sci.*, **29**, 207–215.

Ma, Y., T. Yao, and J. Wang, 2006: Experimental study of energy and water cycle in Tibetan Plateau - The progress introduction on the study of GAME/Tibet and CAMP/Tibet. *Plateau Meteorology* (in Chinese), **25**, 344–351.

Ma, Y., S. Kang, L. Zhu, B. Xu, L. Tian, and T. Yao, 2008: Tibetan observation and research platform (TORP): Atmosphere-land interaction over a heterogeneous landscape. *Bull. Amer. Meteor. Soc.*, **89**, 1487–1492.

Ma, Y., and Coauthors, 2009: Recent advances on the study of atmosphere-land interaction observations on the Tibetan Plateau. *Hydrol. Earth Syst. Sci.*, **13**, 1103–1111.

Mosbrugger, V., and E. Appel, 2012: Research on plateau and climate evolution and geo-ecosystems of the Tibetan Plateau and Central Asia. *Newsletter of the DFG Priority Programme 1372*, No. 1, pp1 (http://www.tip.uni-tuebingen.de/).

Nan, S., P. Zhao, S. Yang, and J. Chen, 2009: Springtime tropospheric temperature over the Tibetan Plateau and evolutions of the tropical Pacific SST. *J. Geophys. Res. Atmos.*, **114**, D10104, doi: 10.1029/2008JD011559.

Qiu, G., H. Li, Y. Zhang, S. Luo, S. Wang, and L. Shang, 2013: Applicability research of planetary boundary layer parameterization scheme in WRF model over the alpine grassland area (in Chinese). *Plateau Meteorology*, **32**, 46–55.

Saraf, N., and G. Beig, 2004: Long-term trends in tropospheric ozone over the Indian tropical region. *Geophys. Res. Lett.*, **31**, L05101, doi: 10.1029/ 2003GL018516.

Su, Z., P. de Rosnay, J. Wen, L. Wang, and Y. Zeng, 2013: Evaluation of ECMWF's soil moisture analyses using observations on the Tibetan Plateau. *J. Geophys. Res. Atmos.*, **118**, 5304–5318.

Su, Z., and Coauthors, 2011: The Tibetan Plateau observatory of plateau scale soil moisture and soil temperature (Tibet-Obs) for quantifying uncertainties in coarse resolution satellite and model products. *Hydrol. Earth Syst. Sci.*, **15**, 2303–2316.

Sugimoto, S., and K. Ueno, 2010: Formation of mesoscale convective systems over the eastern Tibetan Plateau affected by plateau-scale heating contrasts. *J. Geophys. Res. Atmos.*, **115**, D16105, doi: 10.1029/2009JD013609.

Tao, S., S. Luo, and H. Zhang, 1986: The Qinghai-Xizang Plateau Meteorological Experiment (QXPMEX) May–August 1979. *Proceedings of International Symposium on the Qinghai-Xizang Plateau and Mountain Meteorology*, Amer. Meteor. Soc., pp 3–13.

Tobo, Y., D. Zhang, Y. Iwasaka, and G. Shi, 2007: On the mixture of aerosols and ice clouds over the Tibetan Plateau: Results of a balloon flight in the summer of 1999. *Geophys. Res. Lett.*, **34**, L23801, doi: 10.1029/2007GL031132.

Ueno, K., H. Fujii, H. Yamada, and L. Liu, 2001: Weak and frequent monsoon precipitation over the Tibetan Plateau. *J. Meteor. Soc. Japan*, **79**, 419–434.

Uyeda, H., and Coauthors, 2001: Characteristics of convective clouds observed by a Doppler radar at Naqu on Tibetan Plateau during the GAME-Tibet IOP. *J. Meteor. Soc. Japan*, **79**, 463–474.

Vernier, J. P., and Coauthors, 2015: Increase in upper tropospheric and lower stratospheric aerosol levels and its potential connection with Asian pollution. *J. Geophys. Res. Atmos.*, **120**, 1608–1619.

Wan, L. F., D. Guo, R. Q. Liu, C. H. Shi, and Y. C. Su, 2017: Evaluation of WACCM3 performance on simulation of the double core of ozone valley over the Qinghai-Xizang in summer. *Plateau Meteorology* (in Chinese), **36**, 57-66.

Wang, J., 1999: Land surface process experiment and interaction study in China-from

HEIFE to IMGRASS and GAME-Tibet/TIPEX (in Chinese). *Plateau Meteorology*, **18**, 280–294.

Wang, M., S. Zhou, and A. Duan, 2012: Trend in the atmospheric heat source over the central and eastern Tibetan Plateau during recent decades: Comparison of observations and reanalysis data. *Chinese Sci. Bull.*, **57**, 548–557.

Wang, Y., 2011: Contrast the simulation result of WRF model to bounder layer observation at southeast Tibetan plateau. Master Thesis, Nanjing University of Information Science & Technology, pp 39–54.

Wang, Y., and Coauthors, 2016: Analysis of land surface parameters and turbulence characteristics over the Tibetan Plateau and surrounding region. *J. Geophys. Res. Atmos.*, **121**, 9540–9560.

Wu, C., and T. Zhou, 2011: Characteristics of cloud radiative forcings over East Asia as simulated by the AGCMs in the CFMIP (in Chinese). *Acta Meteor. Sin.*, **69**, 381–399.

Wu, G. X., and Coauthors, 2007: The Influence of the mechanical and thermal forcing of the Tibetan Plateau on the Asian climate. *J. Hydrometeorology*, **8**, 770–789.

Wu, G. X., and Y. Zhang, 1998: Tibetan plateau forcing and the timing of the monsoon onset over South Asia and the South China Sea. *Mon. Wea. Rev.*, **126**, 913–927.

Wu, G. X., H. Zhuo, Z. Wang, and Y. Liu, 2016: Two types of summertime heating over the Asian large-scale orography and excitation of potential vorticity forcing I. Over Tibetan Plateau. *Science China Earth Sciences,* **59**, 1996–2008.

Xu, X., and Coauthors, 2008a: A New Integrated Observational System over the Tibetan Plateau (NIOST). *Bull. Amer. Meteor. Soc.*, **89**, 1492–1496.

Xu, X., and Coauthors, 2014: An important mechanism sustaining the atmospheric "water tower" over the Tibetan Plateau. *Atmos. Chem. Phys.*, **14,** 11287–11295.

Xu, X., and Coauthors, 2016: Climate modulation of the Tibetan Plateau on haze in China. *Atmos. Chem. Phys.*, **16,** 1365–1375.

Xu, X., C. Lu, X. Shi, and S. T. Gao, 2008b: World water tower: An atmospheric perspective. *Geophys. Res. Lett.*, **35**, 525–530.

Yan, Y., Y. Liu, and J. Lu, 2016: Cloud vertical structure, precipitation, and cloud radiative effects over Tibetan Plateau and its neighboring regions. *J. Geophys. Res. Atmos.*, **121**, doi: 10.1002/2015JD024591.

Yang, K., and X. Guo, 2011: On the climatology and trend of the atmospheric heat source over the Tibetan Plateau: An experiments-supported revisit. *J. Climate*, **24**, 1525–1541.

Yang, K., and Coauthors, 2013: A multiscale soil moisture and freeze–thaw monitoring network on the Third Pole. *Bull. Amer. Meteor. Soc.*, **94**, 1907–1916.

Ye, D., and Y. Gao, 1979: The Meteorology of the Qinghai-Xizang Plateau (in Chinese). Science Press, Beijing, 1– 278 pp.

Zeng, Y., Z. Su, R. V. der Velde, L. Wang, K. Xu, X. Wang, and J. Wen, 2016: Blending satellite observed, model simulated, and in situ measured soil moisture over Tibetan Plateau. *Remote Sensing*, **8**, 268, doi: 10.3390/rs8030268.

Zhang, G., F. Chen, and Y. Gan, 2016: Assessing uncertainties in the Noah-MP ensemble simulations of a cropland site during the Tibet Joint International Cooperation program field campaign. *J. Geophys. Res. Atmos.*, **121**, doi: 10.1002/2016JD024928.

Zhang, R., T. Koike, X. Xu, Y. Ma, and K. Yang, 2012: A China-Japan cooperative JICA atmospheric observing network over the Tibetan Plateau (JICA/Tibet Project): An overviews. *J. Meteor. Soc. Japan*, **90C**, 1–16.

Zhao, P., L. X. Chen, 2000a: Calculation of solar albedo and radiation equilibrium over the Qinghai-Xizang Plateau and analysis of their climate features. *Adv. Atmos. Sci.*,, 17, 140-156.

Zhao, P., L. X. Chen, 2000b: Study on climatic features of surface turbulent heat exchange coefficients and surface thermal sources over the Qinghai-Xizang Plateau. *Acta Meteor. Sin.* (currently known as *J. Meteor. Res.*), **14**, 13–29.

Zhao, P., and L. X. Chen, 2001a: Climatic features of atmospheric heat source/sink over the Qinghai-Xizang (Tibetan) Plateau in 35 years and its relation to rainfall in China. *Sci. China Ser D-Earth Sci.*, **44**, 858–864.

Zhao, P., and L. X. Chen, 2001b: Interannual variability of atmospheric heat source/sink over the Qinghai-Xizang (Tibetan) Plateau and its relation to circulation. *Adv. Atmos. Sci.*, **18**, 106–116.

Zhao, P., B. Wang, and X. J. Zhou, 2012: Boreal summer continental monsoon rainfall and hydroclimate anomalies associated with the Asian–Pacific Oscillation. *Clim. Dyn.*, **39**, 1197–1207.

Zhao, P., X. D. Zhang, Y. F. Li, and J. M. Chen, 2009: Remotely modulated tropical–North Pacific ocean–atmosphere interactions by the South Asian high. *Atmos. Res.*, **94**, 45–60,

Zhao, P., Z. J. Zhou, and J. P. Liu, 2007: Variability of Tibetan spring snow and its associations with the hemispheric extratropical circulation and East Asian summer monsoon rainfall: An observational investigation. *J. Climate*, **20**, 3942–3955.

Zheng, D., and Coauthors, 2015a: Augmentations to the Noah model physics for application to the Yellow River source area. Part I: Soil water flow. *J. Hydrometeorology*, **16**, 2659–2676.

Zheng, D., and Coauthors, 2015b: Augmentations to the Noah model physics for application to the Yellow River source area. Part II: Turbulent heat fluxes and soil heat transport. *J. Hydrometeorology*, **16**, 2677–2694.

Zheng, D., and Coauthors, 2016: Impacts of Noah model physics on catchment-scale runoff simulations. *J. Geophys. Res. Atmos.*, **121**, 807–832.

Zheng, D., R. van der Velde, Z. Su, M. Booij, A. Hoekstra, and J. Wen, 2014: Assessment of roughness length schemes implemented within the Noah land surface model for high-altitude regions. *J. hydrometeorology*, **15**, 921–937.

Zheng, D., R. van der Velde, Z. Su, J. Wen, M. Booij, A. Hoekstra, and X. Wang, 2015c: Under-canopy turbulence and root water uptake of a Tibetan meadow ecosystem modeled by Noah-MP. *Water Resour. Res.*, **51**, 5735–5755.

Zhou, X., P. Zhao, J. Chen, L. X. Chen, and W. L. Li, 2009: Impacts of thermodynamic processes over the Tibetan Plateau on the Northern Hemispheric climate. *Sci. China Ser D-Earth Sci.*, **52**, 1679–1693.

Zhou, X., C. Luo, W. L. Li, and J. Shi, 1995: Variations of total ozone amount in China and the ozone low center over Tibetan Plateau (in Chinese). *Chinese Sci. Bull.*, **40**, 1396–1398.

Zhu, B., X. Hou, and H. Kang, 2016: Analysis of the seasonal ozone budget and the impact of the summer monsoon on the northeastern Qinghai-Tibetan Plateau. *J. Geophys. Res. Atmos.*, **121**, 2029–2042.

Zhu, X., Y. Liu, G. X. Wu, 2012: An assessment of summer sensible heat flux on the Tibetan Plateau from eight data sets. *Sci. China Earth Sci.*, 2012, **55**, 779–786.

Zhuo, H., Y. Liu, and J. Jin, 2016: Improvement of land surface temperature simulation over the Tibetan Plateau and the associated impact on circulation in East Asia. *Atmos. Sci. Lett.*, **17**, 162–168.

TABLE 1. Measurements of soil moisture and temperature and PBL elements.

Observation name	Description	Number of instruments used in TIPEX-III
Plateau-scale network for soil moisture	The DZN3 automatic soil water observation instrument (with an accuracy of 2.5% volume water content, and made by the China Huayun Group) has one data logger and five sensors at each site. Five sensors are inserted into soil at depths of 10, 20, 30, 40, and 50 cm. This network consists of 46 sites. The observational data are recorded every hour.	46 sets
Regional-scale network for soil moisture and temperature	The 5TM ECH_2O soil moisture observation instrument (with an accuracy of 2% volume water content and 1°C, and made by Decagon, USA) has one data logger and five sensors at each site. Five sensors are inserted into soil at depths of 2, 5, 10, 20, and 30 cm for soil moisture and temperature measurement. The observational data are recorded every ten min.	90 sets
PBL tower measurement systems	One 20-m-high tower has one 020C wind direction sensor (with an accuracy of 3º, and made by Met One, USA) at a height of 20 m, five 010C wind speed sensors (with an accuracy of 0.07 m s^{-1}, made by Met One, USA), five HMP155A air temperature (*T*) and humidity (*RH*) sensors (with an accuracy of 0.226°C-0.0028×T when -80°C<T<20°C and 0.055°C+0.0057×T when 20°C<T<60°C, and an accuracy of 1% when 0<RH<90% and 1.7% when 90%<RH<100%; and made by Campbell Scientific, USA) at heights of about 1.5 m, 2 m, 4 m, 10 m, and 20 m, and one SI-111 surface temperature sensor (with an accuracy of 0.1°C when -10°C<T<65°C and 0.3°C when -40°C<T<70°C, and made by Campbell Scientific, USA) at 0 cm. One 10-m-high tower has the same instruments as the 20-m-high tower but with one wind direction sensor at a height of 10 m, and four wind speed, air temperature, and humidity sensors at heights of about 1.5 m, 2 m, 4 m, and 10 m. The 20-m towers are at Shiquanhe (80.08°E, 32.5°N, 4281 m), Gaize (84.42°E, 32.15°N, 4416 m), Namucuo (91°E, 30.78°N, 4730 m), Naqu (91.9°E, 31.62°N, 4508 m), Anduo (91.63°E, 32.23°N, 4695 m), Linzhou (91.27°E, 29.9°N, 3744 m), Linzhi (94.73°E, 29.77°N, 2992 m), Tuotuohe (92.43°E, 34.21°N, 4533 m), Maqu (102.08°E, 34°N, 3471 m), Litang (100.27°E, 30°N, 3948 m), Dali (100.18°E, 25.7°N, 1990 m), and Wenjiang (103.83°E, 30.7°N, 540 m). The 10-m towers are at Bange (90.03°E, 31.42°N, 4700 m), Nierong (92.3°E, 32.12°N, 4623 m), Jiali (93.23°E, 30.65°N, 4509 m), and Biru (93.15°E, 31.67°N, 4408 m). The observational data are recorded every 10 s.	Twelve 20-m and four 10-m towers
Integrated sonic turbulent wind and CO_2/H_2O flux measurement system at PBL site	The instrument (made by Campbell Scientific, USA) has one 3-D sonic anemometer and one CO_2/H_2O open-path gas analyzer for measuring wind speed (with an accuracy of 8.0 cm s^{-1} for horizontal velocity, and 4.0 cm s^{-1} for vertical velocity), temperature (with an accuracy of 0.15°C when temperature is 30°C to 50°C), and CO_2 and H_2O fluxes (with accuracy of 0.2 mg m^{-3} and 0.004g m^{-3}, respectively) at 2 m. The observational data are recorded every 0.1 s.	16 sets
Surface radiation measurement at PBL site	One CNR radiation sensor (with an accuracy of 1%, and made by Kipp and Zonen, the Netherlands) measures downward and upward shortwave and longwave radiation at 1.5 m. The observational data are recorded every 10 s.	16 sets
Soil moisture and temperature measurement system at PBL site	Each set (made by Campbell Scientific, USA) has five 109 soil temperature probes (with accuracy of 0.20°C, 0.18°C, 0.15°C, 0.13°C, and 0.10°C when temperature is -40°C to -30°C, -30°C to -20°C, -20°C to -10°C, -10°C to 0°, and 0° to 70°C, respectively), and five CS616 soil moisture sensors (with an accuracy of 0.1% volume water content) which are inserted at depths of 5, 10, 20, 50, and 100 cm. The observational data are recorded every 10 s.	16 sets

Soil heat flux measurement system at PBL site	One HFP01 soil heat sensor (with an accuracy of 2.5% volume water content, and made by Hukseflux, the Netherlands) is inserted at 5 cm. The observational data are recorded every 10 s.	16 sets
Rainfall measurement at PBL site	One TE525MM rain gauge (with an accuracy of 1–2% h^{-1} when rainfall is 50 mm h^{-1}, and made by Campbell Scientific, USA) automatically records rain intensity every min.	16 sets

TABLE 2. Sounding system for the atmospheric profiles.

Instrument name		Description	Number of instruments used in TIPEX-III
	GPZ1 automatic sounding system	Made by Great Bridge Machine Limited Company of Nanjing, China. Each installation provides balloons, sounders, and hydrogen for up to 24 observations. When this system works, it can automatically conduct gas inflation, launches, and data collection from the surface to 35 km, up to 24 times through presetting the time and instructions for each operation. A system is located at Shiquanhe (80.08°E, 32.5°N, 4281 m), Gaize (84.42°E, 32.15°N, 4416 m), and Shenzha (88.63°E, 30.95°N, 4672 m), respectively.	3 sets
	QDQ2-1 hydrogen generation equipment	Made by Great Bridge Machine Limited Company of Nanjing, China. Generates hydrogen through water electrolysis.	3 sets
	XGP-3 GZ sounder	Made by Great Bridge Machine Limited Company of Nanjing, China, and measures wind speed, wind direction, pressure, air temperature, and relative humidity (with accuracy of 0.5 m s^{-1}, 10º, 0.5 hPa, 0.3ºC, and 10%, respectively). The observational data are recorded every second.	Disposable consumables
	Vaisala RS 92 radiosonde	Made by Vaisala, Finland, and measures profiles of pressure (p), temperature, relative humidity, and wind, with an accuracy of 0.1~0.3 hPa when p>100 hPa, and 0.1~0.04 hPa when p <100 hPa for pressure, 0.3°C when p>100 hPa and 0.6°C when p<100 hPa for temperature, 3% when T>-40°C and 5% when T<-40°C for relative humidity, and 0.5 m s^{-1} for wind. The observational data are recorded every 2s.	Disposable consumables

TABLE 3. Ground-based radar measurements of cloud-precipitation physical features.

Instrument name and manufacturer		Description (with accuracy in brackets)	Number of instruments used in TIPEX-III
	C-band continuous-wave radar (made by Anhui Sun-create Electronics Limited Company, China)	Measures echo intensity (1 dB), radial velocity (1 m s^{-1}), velocity spectrum width (0.1 m s^{-1}), and has a spatial resolution of 15–30 m and a temporal resolution of 2–3 s.	1 set
	C-band dual polarization radar (made by the Anhui Sun-create Electronics Limited Company, China)	Measures echo intensity (1 dB), radial velocity (1 m s^{-1}), velocity spectrum width (0.1 m s^{-1}), differential depolarization factor (0.2 dB), specific differential phase (2°), and correlation coefficient (0.01), and has spatial resolutions of 0.3 km and 1°, and a temporal resolution of 6 min.	1 set
	Ka-band millimeter-wave cloud radar (made by the 23rd Institute of China Aerospace Science and Technology Corporation)	Measures echo intensity of cloud (1 dB), radial velocity (1 m s^{-1}), velocity spectrum width (0.5 m s^{-1}), depolarization factor (1 dB), function of power spectrum density (1 dB), and has a spatial resolution of 30 m and a temporal resolution of 2 s.	1 set
	Ka-band millimeter-wave cloud radar (made by the Xian Huateng Microwave Company, China)	Measures echo intensity of cloud (1 dB), radial velocity (1 m s^{-1}), velocity spectrum width (1 m s^{-1}), function of power spectrum density (1 dB), and has a spatial resolution of 30 m and a temporal resolution of 1 min.	1 set
	Lidar for water vapor and cloud observation (made by the Ocean University of China, China)	Measures water vapor profile (5%) and cloud base height (10 m), and has a spatial resolution of 3.75 m and a temporal resolution of 16 s.	1 set
	MP-3000A microwave radiometer (made by Radiometrics Company, USA)	Measures brightness temperature (0.2°C), and has a temporal resolution of 2 min, which may be used to retrieve atmospheric liquid water content, atmospheric water vapor, and temperature profiles.	1 set
	MRR-2 micro-rain radar (made by METEK Meteorologische Messtechnik GmbH, Germany)	Measures echo intensity (1 dB) and rainfall (0.01 mm h^{-1}), and has a spatial resolution of 50–200 m and a temporal resolution of 1 min.	1 set
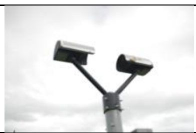	PS32 disdrometer (made by Vaisala, Finland)	Measures raindrop spectrum (32 grades), and has a temporal resolution of 1 min.	3 sets
	Vaisala CL31 ceilometer (made by Vaisala, Finland)	Measures cloud base height and PBL (5 m), and has a spatial resolution of 5 m and a temporal resolution of 16 s.	1 set

TABLE 4. Airborne measurements of cloud-precipitation physical features.

Instrument name and manufacturer		Description	Number of instruments used in TIPEX-III
	King Air 350 ER	Equipped with GPS, flight altitude below 10000 m, flying time of 5 hours, and flight speed between 280 km h^{-1} and 560 km h^{-1}. Operated by the Beijing Weather Modification Office.	1 set
	Aircraft integrated meteorological measurement system (AIMMS-20) (made by Aventech Research Inc, Canada)	Measures temperature, humidity, horizontal wind, vertical wind speed (with an accuracy of 0.3°C, 2.0%, 0.5 m s^{-1}, and 0.75 m s^{-1}, respectively), latitude, longitude, height, and GPS (with an accuracy of 10 m). The observational data are recorded every 0.05 s.	1 set
	Fast cloud droplet probe (FCDP) (made by Stratton Park Engineering Company, USA)	Measures the size and number concentration of cloud particles, with an accuracy of 2 μm. The observational data are recorded every 0.025 s.	1 set
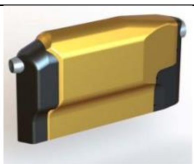	Three-view cloud particle imager (3V-CPI) (made by Stratton Park Engineering Company, USA)	Consists of a cloud particle Imager (CPI) with a resolution of 3.2 μm, and a two-dimensional stereo (2D-S) probe with a measurement range between 10 μm and 1280 μm and an imaging frequency of a 400 frame per second.	1 set
	Version 3 high volume precipitation spectrometer (HVPS-3) (made by Stratton Park Engineering Company, USA)	Measures the spectrum and image of precipitation particles, with a measurement range between 150 μm and 19200 μm. Particles are fully imaged with a sample volume of 310 l s^{-1} at an airspeed of 100 m s^{-1}.	1 set
	Nevzorov liquid water content/total water content (LWC/TWC) sensor (made by Skytech Research Ltd., UK)	A combined sensor for liquid water and total water content, with a measurement range between 0.005 g m^{-3} and 3 g m^{-3}. The observational data are recorded every second.	1 set
	Goodrich model 102LJ2AG (made by Goodrich Corporation, USA)	Measures total air temperature (TAT) with an accuracy of 0.5°C, in which the TAT measurement is a component of the airstream, and it reflects an effect of bringing airflow to rest. It is the only way to accurately measure outside air temperature above 200 KIAS (Knots-Indicated Air Speed). The observational data are recorded every second.	1 set
	Goodrich model 0871LM5 icing probe detector (made by Goodrich Corporation, USA)	Detects the presence of icing conditions, and is sensitive to less than 0.001 inches of ice. The observational data are recorded every second.	1 set

TABLE 5. Balloon-borne and ground-based measurements of ozone, aerosol, and water vapor in the troposphere and stratosphere.

Instrument name and manufacturer	Description	Number of instruments used in TIPEX-III
 ECC 6A (En-Sci) ozonesonde (made by Droplet Measurement Technologies, USA) with Vaisala RS 92 radiosonde (made by Vaisala, Finland)	Measures profiles of pressure, temperature, relative humidity, wind, and ozone concentration (with an accuracy of 5–10% up to 30 km altitude). The observational data are recorded every 2s.	Disposable consumables
 Cryogenic frost hydrometer (CFH) (made by Droplet Measurement Technologies, USA)	Measures profiles of water vapor from the surface to about 28 km, with an uncertainty of <4% in the troposphere, and <9% in the stratosphere. The Imet–radiosonde is used as a platform of data transmission, and the observational data are recorded every 1.2 s.	Disposable consumables
 Compact optical backscatter aerosol detector (COBALD) (made by Eidgenössische Technische Hochschule Zürich, Switzerland)	Measures light backscattering ratios of molecules, aerosols, and ice particles at wavelengths of 455 nm and 940 nm in the UT-LS, with an uncertainty of about 5% (<1% in the UT-LS), and works with the Imet-radiosonde-CFH platform. The observational data are recorded every 1.2 s.	Disposable consumables
 Micro-pulse backscatter lidar (MPL-4B) (made by Sigma Space Corporation, USA)	Measures profiles of aerosol backscattering ratio at 532 nm, with a vertical resolution of 30 m. The observational data are recorded every 30 s.	1 set
 MKII Brewer ozone spectrophotometer (made by Kipp and Zonen, the Netherlands)	Measures total column ozone and solar spectral UVB, with an uncertainty of <1% for ozone and an accuracy of 5–10% for spectral UVB irradiance. The observational data are recorded every 5 min for ozone and every 8 min for solar spectral UVB (with a given solar zenith angle).	3 sets

TABLE 6. The median values of C_d (×10^{-3}) and C_h (×10^{-3}) for the eleven TIPEX-III sites under neutral conditions (Wang et al. 2016).

Site	Anduo	Bange	Biru	Dali	Jiali	Linzhi	Namucuo	Naqu	Nierong	Shiquanhe	Wenjiang
C_h	2.4	2.7	3.4	4.5	3.8	6.0	2.2	2.8	3.2	2.4	4.7
C_d	2.9	3.4	10.1	11.6	10.5	8.0	3.8	4.4	3.8	9.6	12.6

Figure captions

FIG. 1. (a) Distribution of 46 newly built (black dot) and CMA operational (red dot) sites for monitoring soil moisture and temperature—boxes represent regional-scale soil moisture and temperature observation networks; (b) distribution of PBL sites (purple stars), a regional PBL network near Naqu (blue solid box), newly built (black dot) and CMA operational (red dot) radiosonde sites, observation areas for cloud-precipitation physical processes (black dashed boxes), new observation sites for ozone, water vapor, and aerosol in the UT-LS (blue hollow triangle), and CMA operational observation sites for atmospheric composition at the land surface (black solid triangle)—the thick, black dashed line indicates the line of aircraft flight from Golmud to Naqu in the summer of 2014; and (c) distribution of 33 sites of the regional-scale soil moisture and temperature observation network over Naqu.

FIG. 2. (a) Daily mean time series of *SH* (W m^{-2}) at the Shiquanhe site (dashed line), and a regional mean of *SH* over six sites of the Naqu regional network (solid line) from August 1 to 31, 2014—bars indicates the maximum and minimum values of *SH* among the six sites; and (b) same as in (a) but for *LH*.

FIG. 3. (a) Cloud particle images (CPI) sampled by airborne CPI and 2D-S for precipitating cumulus clouds at temperatures between -2.5°C and -3.5°C at Naqu on July 21, 2014, in which 2D-S is the two-dimensional stereo (see Table 4); (b) the mean raindrop size distribution of 112 rainfall events near Naqu in July and August, 2014, and the fitted M-P (with N_0=8000 m^{-3} mm^{-1}, R=1.16 mm h^{-1}) and Γ (with N_0=17349.34 m^{-3}, μ=4.03, Λ=6.95 mm^{-1}) raindrop size distributions (Chang and Guo 2016); and (c) the relationship between concentration ($l^{-1}\mu m^{-1}$) and diameter (μm) of cloud particles at Naqu on 21 July 2014, in which FCDP is the

fast cloud droplet probe and HVPS is the high volume precipitation spectrometer (see Table 4).

FIG. 4. (a) The vertical profiles of averaged temperature (°C; black) over 31 observations, averaged ozone concentration (mPa; red) over 31 ozonesondes, and averaged water vapor concentration (ppm; blue) over 11 observations at Linzhi in June and July, 2014; (b) the vertical profile of ozone concentration difference (mPa) between Linzhi and New Delhi (28.3°N, 77.07°E), India, in which the ozone concentration in New Delhi comes from Saraf and Beig (2004); (c) variations of the polar tropopause height as a function of time at Gaize from July 8 to August 31, 2014 (Hong et al. 2016); and (d) same as in (c) but for the tropical tropopause height (Hong et al. 2016).

FIG. 5. (a) A diagram of the mechanism for sustaining the “atmospheric water tower” over the TP, in which Q1/Q2 is the apparent heat source/moisture sink, the CISK (1)/(2) indicates the first/second ladder of CISK-like processes on the TP slope/main platform, and $\nabla \cdot \mathrm{V}$ is the horizontal convergence/divergence of air mass (Xu et al. 2014); (b) the root-mean-square difference of 24-hour forecast rainfall (mm day^{-1}) between experiments with and without intensive observational data over the western TP during June 1 to August 31, 2015, in which black dots are the rain-gauge stations; (c) the three cross sections of the regressed vertical circulation (black) and eddy temperature (°C; color shading) against the interannual component of a summer (June-July-August) TP surface air temperature index along 85°E, 55°N, and 175°W, respectively, using the 1948–2015 NCEP reanalysis, in which black shaded areas denote terrain (Liu et al. 2017); (d) summer 850-hPa wind anomalies (m s^{-1}) forced by an increased TP heating in the NCAR Community Atmosphere Model version 3 (CAM3) with prescribed monthly SST

(CAM3_Tree minus CAM3_Bare), in which CAM3_Tree/CAM3_Bare has a surface type of broad leaf evergreen tropical tree/bare soil (corresponding to lower/higher surface albedo) over the TP (Liu et al. 2017) and the last ten-year outputs of a 20-year model integration are analyzed; (e) same as in (d) but for rainfall (mm day^{-1}; black dotes are significant at the 90% confidence level); and (f) same as in (e) but for surface air temperature (^{o}C).

(a)

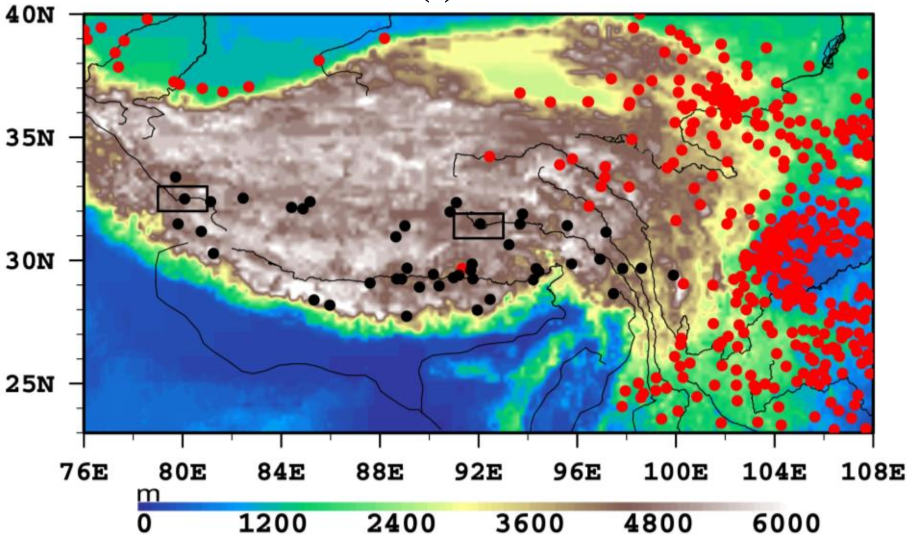

40N
35N
30N
25N
76E
80E
84E
88E
92E
96E
100E
104E
108E
m
0
1200
2400
3600
4800
6000

(b)

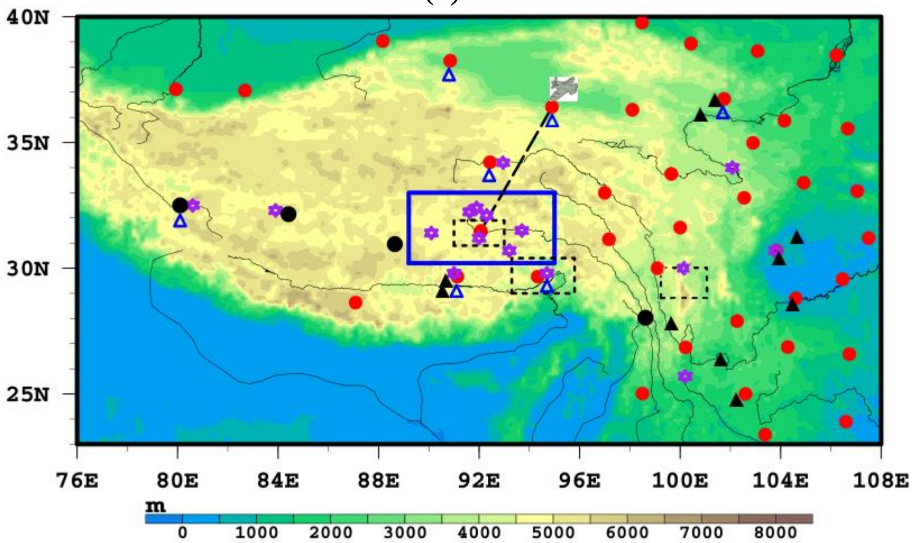

40N
35N
30N
25N
76E
80E
84E
88E
92E
96E
100E
104E
108E
m
0
1000
2000
3000
4000
5000
6000
7000
8000

(c)

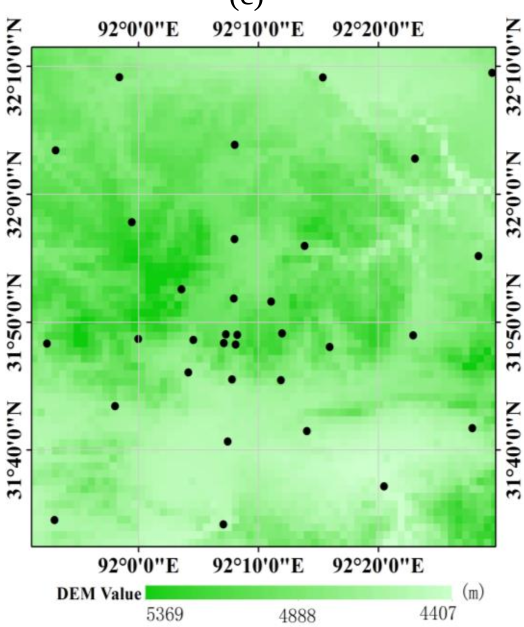

92°0'0"E
92°10'0"E
92°20'0"E
32°10'0"N
32°0'0"N
31°50'0"N
31°40'0"N
DEM Value
(m)
5369
4888
4407

FIG. 1. (a) Distribution of 46 newly built (black dot) and CMA operational (red dot) sites for monitoring soil moisture and temperature—boxes represent regional-scale soil moisture and temperature observation networks; (b) distribution of PBL sites (purple stars), a regional PBL network near Naqu (blue solid box), newly built (black dot) and CMA operational (red dot) radiosonde sites, observation areas for cloud-precipitation physical processes (black dashed boxes), new observation sites for ozone, water vapor, and aerosol in the UT-LS (blue hollow triangle), and CMA operational observation sites for atmospheric composition at the land surface (black solid triangle)—the thick, black dashed line indicates the line of aircraft flight from Golmud to Naqu in the summer of 2014; and (c) distribution of 33 sites of the regional-scale soil moisture and temperature observation network over Naqu.

(a)

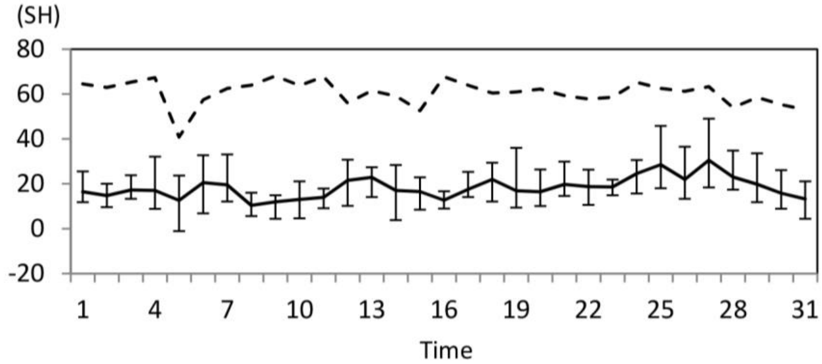

(b)

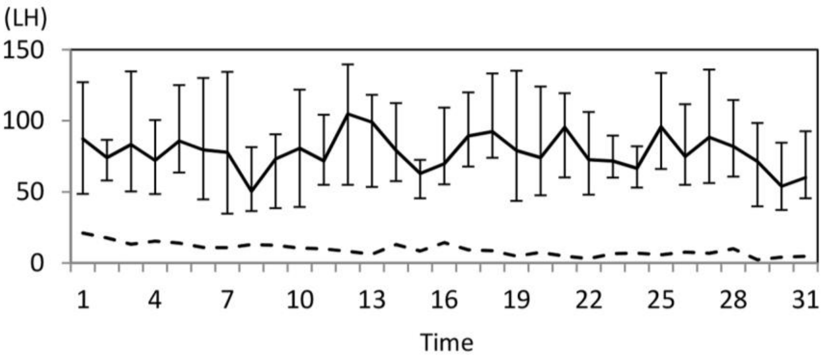

FIG. 2. (a) Daily mean time series of *SH* (W m^{-2}) at the Shiquanhe site (dashed line), and a regional mean of *SH* over six sites of the Naqu regional network (solid line) from August 1 to 31, 2014—bars indicates the maximum and minimum values of *SH* among the six sites; and (b) same as in (a) but for *LH*.

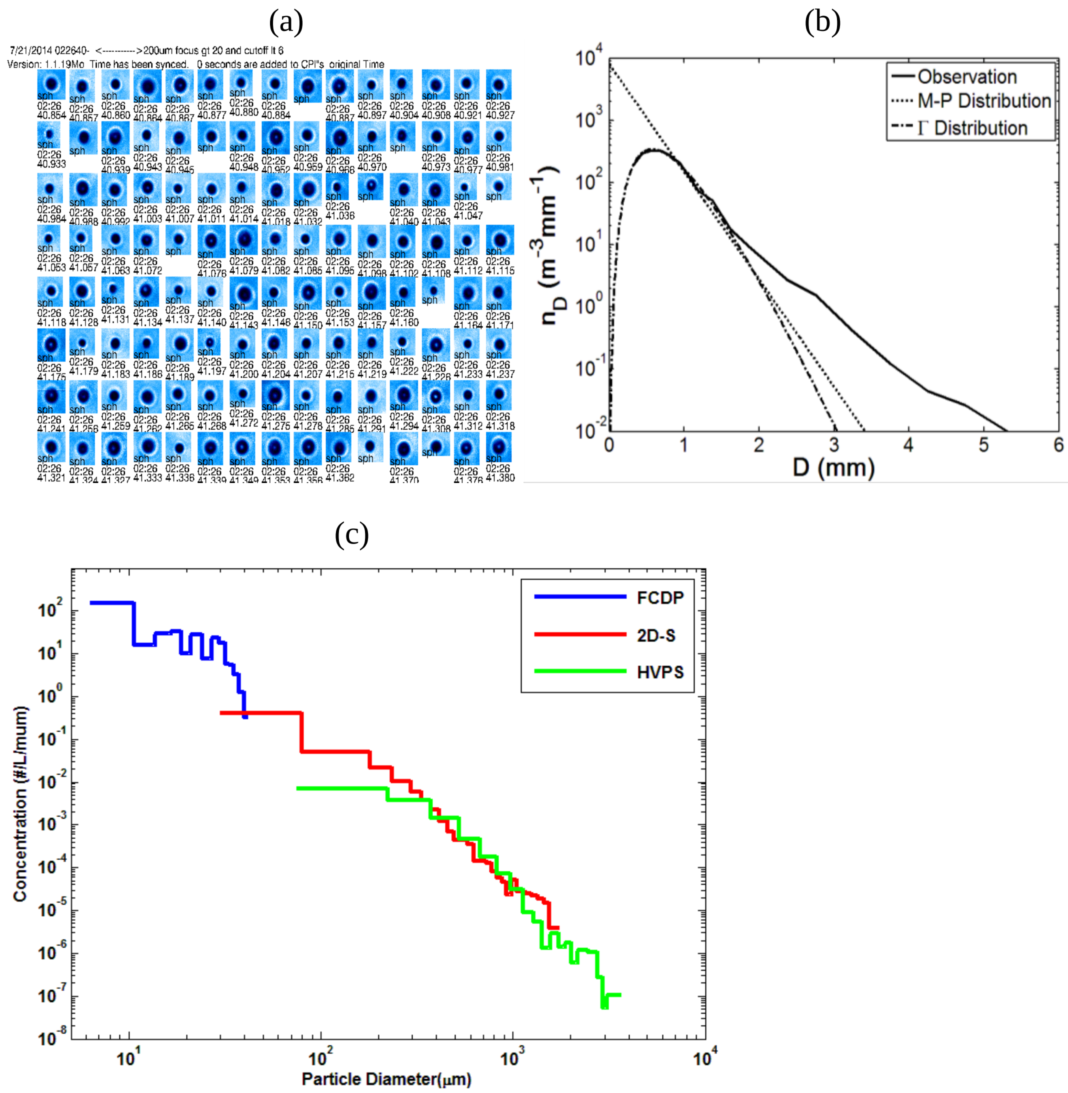

FIG. 3. (a) Cloud particle images (CPI) sampled by airborne CPI and 2D-S for precipitating cumulus clouds at temperatures between -2.5°C and -3.5°C at Naqu on July 21, 2014, in which 2D-S is the two-dimensional stereo (see Table 4); (b) the mean raindrop size distribution of 112 rainfall events near Naqu in July and August, 2014, and the fitted M-P (with N_0=8000 m^{-3} mm^{-1}, R=1.16 mm h^{-1}) and Γ (with N_0=17349.34 m^{-3}, μ=4.03, Λ=6.95 mm^{-1}) raindrop size distributions (Chang and Guo 2016); and (c) the relationship between concentration ($l^{-1}μm^{-1}$) and diameter (μm) of cloud particles at Naqu on 21 July 2014, in which FCDP is the fast cloud droplet probe and HVPS is the high volume precipitation spectrometer (see Table 4).

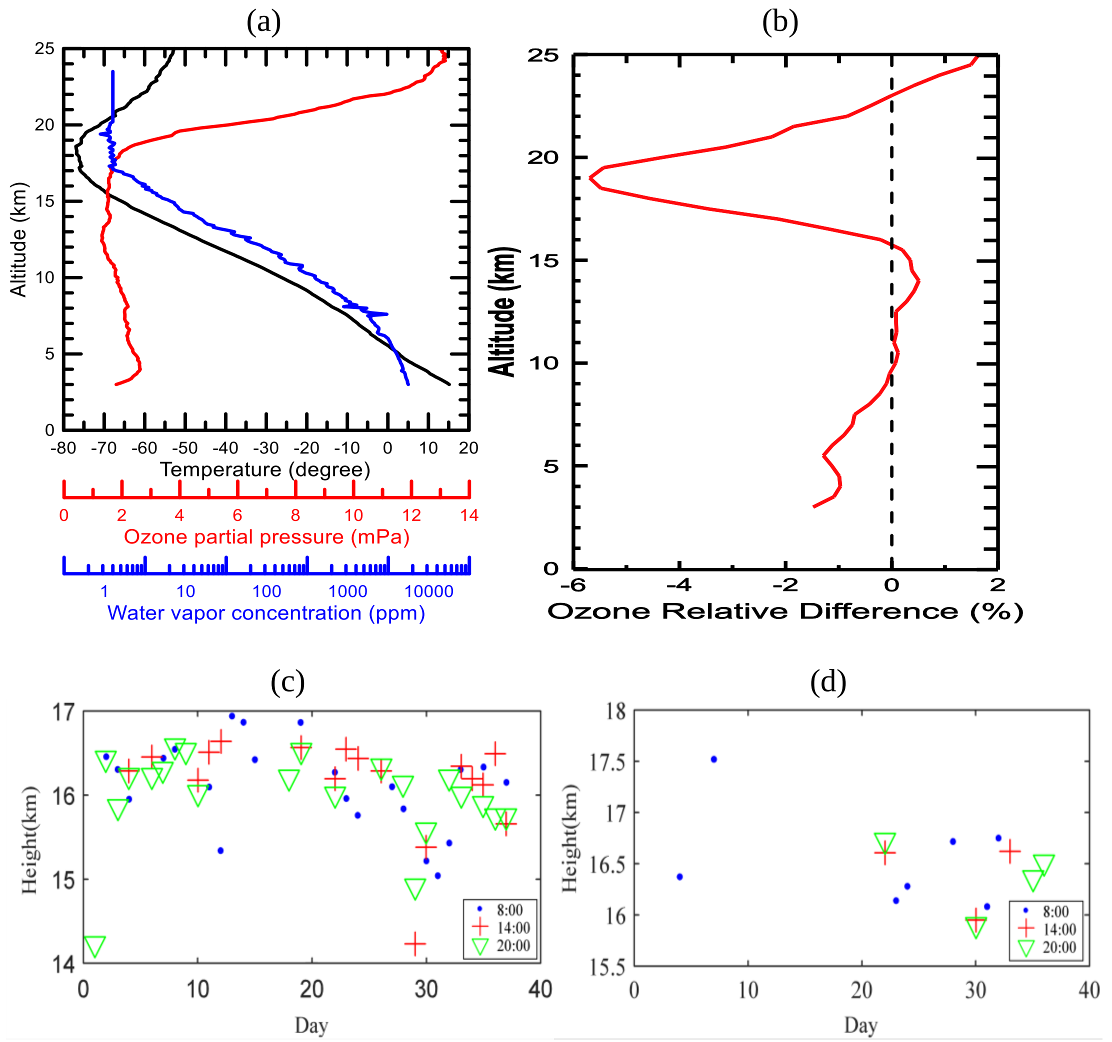

FIG. 4. (a) The vertical profiles of averaged temperature (°C; black) over 31 observations, averaged ozone concentration (mPa; red) over 31 ozonesondes, and averaged water vapor concentration (ppm; blue) over 11 observations at Linzhi in June and July, 2014; (b) the vertical profile of ozone concentration difference (mPa) between Linzhi and New Delhi (28.3°N, 77.07°E), India, in which the ozone concentration in New Delhi comes from Saraf and Beig (2004); (c) variations of the polar tropopause height as a function of time at Gaize from July 8 to August 31, 2014 (Hong et al. 2016); and (d) same as in (c) but for the tropical tropopause height (Hong et al. 2016).

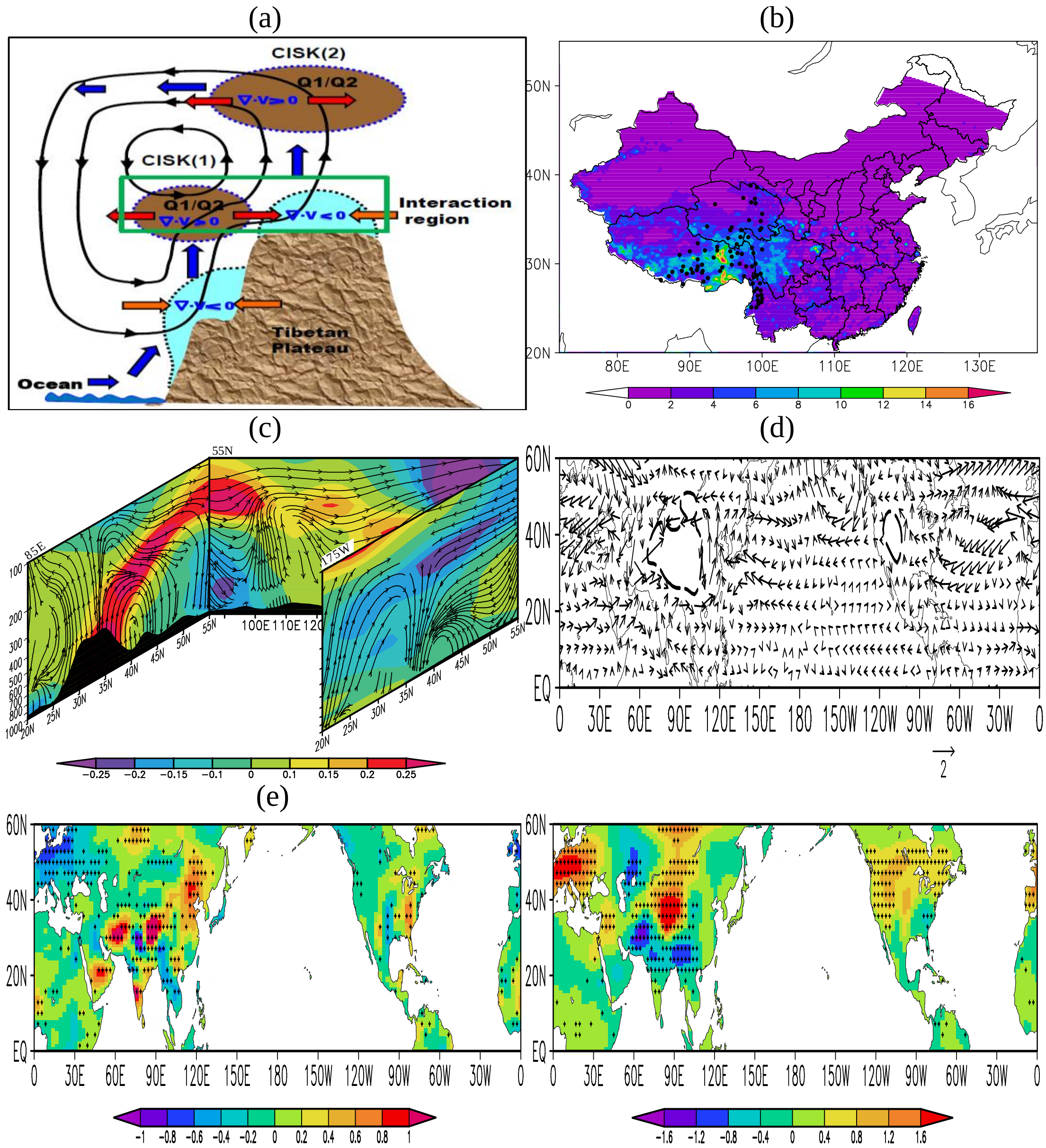

FIG. 5. (a) A diagram of the mechanism for sustaining the “atmospheric water tower” over the TP, in which Q1/Q2 is the apparent heat source/moisture sink, the CISK (1)/(2) indicates the first/second ladder of CISK-like processes on the TP slope/main platform, and ∇ · V is the horizontal convergence/divergence of air mass (Xu et al. 2014); (b) the root-mean-square difference of 24-hour forecast rainfall (mm day^{-1}) between experiments with and without intensive observational data over the western TP during June 1 to August 31, 2015, in which black dots are the rain-gauge stations; (c) the three cross sections of the regressed vertical circulation (black) and eddy

temperature (°C; color shading) against the interannual component of a summer (June-July-August) TP surface air temperature index along 85°E, 55°N, and 175°W, respectively, using the 1948–2015 NCEP reanalysis, in which black shaded areas denote terrain (Liu et al. 2017); (d) summer 850-hPa wind anomalies (m s^{-1}) forced by an increased TP heating in the NCAR Community Atmosphere Model version 3 (CAM3) with prescribed monthly SST (CAM3_Tree minus CAM3_Bare), in which CAM3_Tree/CAM3_Bare has a surface type of broad leaf evergreen tropical tree/bare soil (corresponding to lower/higher surface albedo) over the TP (Liu et al. 2017) and the last ten-year outputs of a 20-year model integration are analyzed; (e) same as in (d) but for rainfall (mm day^{-1}; black dotes are significant at the 90% confidence level); and (f) same as in (e) but for surface air temperature (^{o}C).